Geotextiles and Geomembranes 46 (2018) 354–365

Contents lists available at ScienceDirect

Geotextiles and Geomembranes

journal homepage: www.elsevier.com/locate/geotexmem

Numerical simulation of compaction-induced stress for the analysis of RS walls under working conditions

S.H. Mirmoradi*, M. Ehrlich

Dept. of Civil Engineering, COPPE, Federal University of Rio de Janeiro, RJ, 21945-970, Brazil

ARTICLE INFO

Keywords:
Geosynthetics
Compaction-induced stress
Numerical modelling
Reinforced soil walls

ABSTRACT

This paper aimed to verify numerical modelling of compaction-induced stress (CIS) for the analysis of geosynthetic-reinforced soil (GRS) walls under working stress conditions. Data from a full-scale well-instrumented GRS wall was used for a numerical analysis. The results from the wall used in this study have already been used for validation in several other numerical modelling studies. Nevertheless, in none of these studies was the real value of CIS specified for the vibrating plate compactor used in the wall employed. In the present study, the real value of CIS is employed. The CIS is modelled using a new procedure presented in this paper in addition to two other procedures found in the literature. The results indicate that when the real value of CIS was simulated using a strip load applied to the top of each backfill layer, the numerical model accurately represented the measurements. The accuracy of the results, however, depends on the width of the strip load used to model the CIS. Nevertheless, as this type of compaction modelling procedure is time consuming, modelling of CIS by applying a distribution load at the top and bottom of each soil layer is suggested as an alternative procedure.

1. Introduction

Compaction may significantly affect the internal stresses of reinforced soil walls. To correctly model the behaviour of these structures, the effect of backfill compaction must be considered. Depending on the magnitude of the induced stress due to backfill compaction and the wall height, the horizontal residual stresses in the reinforced soil mass may be much greater than those from a geostatic origin, which may lead to a significant increase in the reinforcement loads. Note that the soil type may also affect this behaviour; high interlocking may lead to higher induced stress due to backfill compaction. Due to these induced stresses, the structure becomes less sensitive to post-construction movements. Surcharge loads may lead to a smaller stress increase in the reinforced soil mass than the induced stresses during construction by backfill compaction. The final effect of this process can be understood as a kind of over-consolidation or pre-loading of the reinforced soil mass that may significantly reduce post-construction movements (Ehrlich and Mitchell, 1995; Ehrlich et al., 2012).

In most of the current design methods for reinforced soil walls, the effect of the compaction-induced stress is not explicitly taken into consideration—e.g. AASHTO (2014) in the USA and BS 8006 (BSI, 2010) in the UK. Note that in RS walls, two different failure conditions may occur: (a) a pullout occurs or the soil may reach its limit condition but the reinforcements do not fail; (b) the reinforcements fail by tension first, followed by the soil. Compaction may lead to a significant increase in reinforcement tension, and this may promote failure by tension or pullout if the reinforcements are not appropriately designed to support those loads. This may specially occur when stiff reinforcements are used (failure type b). This type of failure cannot be explicitly considered by the AASHTO and BS design methods that are not for working stress conditions. These procedures assume that enough lateral deformation may occur resulting in relaxation of compaction residual stress without failure of the reinforcements (failure type a).

Mirmoradi and Ehrlich (2016) investigated the prediction capability of the AASHTO simplified method, considering different controlling factors on reinforced soil (RS) walls, including the compaction-induced stress. It was shown that this method may underestimate the maximum reinforcement loads for walls upon which a high compaction-induced stress is applied. There are some methods, however, which explicitly consider the effect of this factor on their calculations (e.g. Ehrlich and Mirmoradi, 2016; Ehrlich et al., 2017). Comparison of the predicted results using these methods showed good agreement with measured reinforcement load data for several full-scale walls containing a range of reinforcement types.

Numerical modelling may be a powerful tool to properly represent field conditions, if boundary conditions, geometry, constitutive models, parameters, and representative modelling procedure are correctly employed. One of the advantages of this method is that it guarantees good

* Corresponding author.
E-mail address: shm@ufrj.br (S.H. Mirmoradi).

https://doi.org/10.1016/j.geotexmem.2018.01.006
Received 18 August 2017; Received in revised form 10 January 2018; Accepted 10 January 2018

parametric analyses in which only one factor may be varied in isolation. Over the last few decades, several numerical studies have been carried out to investigate the influence of different controlling factors on the behaviour of reinforced soil structures. Examples include: Hermann and Al-Yassin (1978), Rowe and Ho (1993), Ho and Rowe (1997), Ling and Leshchinsky (2003), Liu and Won (2009), Gu et al. (2017), among others. Nevertheless, the effect of compaction-induced stress has rarely been considered in these analyses. Among the studies in which the compaction-induced stress was numerically modelled, two procedures have been used for the simulation (hereafter referred to as procedures type I and type II):

Type I) A uniform vertical stress applied only to the top of each backfill layer, as the wall was modelled from the bottom up (e.g. Hatami and Bathurst, 2005; Guler et al., 2007; Ambauen et al., 2015; Yu et al., 2016, 2017).

Type II) An equally distributed load at the top and bottom of each soil layer (e.g. Mirmoradi and Ehrlich, 2015a; Scotland et al., 2016).

Mirmoradi and Ehrlich (2014, 2015a,c) stated that a model of compaction procedure type II could properly simulate the effects of compaction observed in the physical model studies. On the other hand, a model of compaction procedure type I overestimated the measurements, and the discrepancy increased with depth and magnitude of the compaction effort. Yu et al. (2016) stated that “there is no obvious advantage of one method over the other on theoretical grounds”. Thus, additional study is required to clarify this discrepancy.

The objective of the present study is to verify a numerical modelling of CIS using data from a full-scale GRS wall under working stress conditions. Note that the results from the wall used in this study (wall 1 built at the Royal Military College of Canada RMC) have already been utilised for validation in several other numerical model studies (e.g. Guler et al., 2007; Hatami and Bathurst, 2005; Mirmoradi and Ehrlich, 2015b; Ambauen et al., 2015). None of those studies, however, has employed the real value of the compaction vertical stress specified for the vibrating plate compactor used on wall 1. In all the aforementioned studies, a compaction stress value of 8 kPa was used in the numerical analyses. However, the specifications of the equipment used for backfill compaction in wall 1 indicate a dynamic contact pressure of 55 kPa. This real specified value of CIS of the equipment used for backfill compaction is employed for the analyses using a new procedure presented in this study for compaction modelling in addition to two other procedures found in the literature.

2. Compaction-induced stress

Duncan and Seed (1986) indicated that the compaction operation may be modelled by load and unload cycles that would induce high horizontal residual stresses in the soil. In the field, the soil backfill goes through a complex stress path because of the various load and unload cycles caused by the passing of compaction equipment. The roller sinks into the soil to a depth sufficient to produce a limit equilibrium condition. Note that the roller-soil contact area varies with the shear resistance and stiffness of the backfill soil that varies with the number of passes. This was simplified by Ehrlich and Mitchell (1994) by assuming only one cycle of load-unload for each layer of backfill. Note that in the modelling of compaction-induced stress-strain, soil parameters representative of the backfill soil at the end of compaction should be used, so that they represent the condition found at the last compaction cycle.

Fig. 1 shows the assumed stress path due to the compaction of the backfill layer by applying a single load-unload stress cycle. In this figure, different stress states were considered, corresponding with four conditions as follows: (1) soil placement; (2) compaction equipment operation; (3) end of compaction; and (4) placement of the next soil layer. Due to the operation of the compaction equipment, the vertical stress increases to the maximum effective vertical stress induced during compaction, $\sigma'_{zc,i}$, and simultaneously the horizontal stresses would increase to their maximum values (point 2). Although after unloading (at the end of the compaction operation) the vertical stress returns to its initial value, σ'_z, (point 3), the same cannot be said to occur for the horizontal stresses, as the soil is not an elastic material. Thus, a residual horizontal stress remains in the soil due to the compaction operation ($\Delta\sigma'_{sx,c}$). The placing of the next layer leads to an increase in vertical stress, and a small variation in horizontal stress (point 4). The residual horizontal stress completely disappears only when the geostatic stress at the top of the soil layer overcomes the value of the vertical stress induced during the compaction operations, $\sigma'_{zc,i}$.

Fig. 2 shows a schematic view of the increase in vertical stress during a roller operation in soil backfill. The vertical stress at the top of each layer during the compaction roller operation may be represented by a strip load, and an elastic solution could be used to represent its evolution with depth. For each soil layer the maximum stress increase during the roller operation occurs at the point of soil-roller contact, and decreases with depth. This depth depends on the width of the load applied for the compaction operation, B. For roller (strip load) and tamper (rectangular load) compactors, the depths of soil in which about 10% of the maximum stress increase would occur during the compaction operation are about six and two times the load width, B, respectively (Lambe and Whitman, 1969).

Ehrlich and Mitchell (1994) stated that “in multilayer construction, the compacted layers are relatively thin, typically 0.15–0.3 m thick, and all points in each soil layer may be assumed to have been driven to the same maximum soil stress state during compaction”. Therefore, it may be assumed that all points are driven to the same vertical induced stress, $\sigma'_{zc,i}$, due to compaction.

It is well known that the lateral strain of the reinforced soil layer, in the direction perpendicular to the face of the wall, reduces the maximum horizontal stress induced by compaction when compared to the maximum stress that would exist in cases where there are no lateral strains. Therefore, the actual maximum horizontal stress induced by compaction is also a function of the reinforcements and facing stiffness (point 3 in Fig. 1). However, the vertical stress induced by compaction may be assumed to be independent from the horizontal strains.

Tables 1 and 2 show the characteristics of various vibrating rollers and vibrating tampers, respectively, which were provided by the producing companies. For plates, the vertical compaction-induced stress, $\sigma'_{zc,i}$, can be assumed to be the average contact pressure at the base of the equipment. The centrifugal forces listed are the maximum vibration amplitude of the rollers. Fig. 3 shows the $\sigma'_{zc,i}$ values of compactor rollers for soil with a specific 18 kN/m^3 weight and various angles of friction, determined using equations developed by Ehrlich and Mitchell (1994). For a cohesionless soil, $\sigma'_{zc,i}$ is given by:

$$\sigma'_{zc,i} = (1 - \upsilon_o)(1 + K_a)(QN_\gamma/\gamma L)^{1/2} \quad (1)$$

where υ_o is the Poisson ratio at rest, K_a is the Rankine active earth pressure, Q is the compactor equipment equivalent static load, L is the roller length, N_γ is the soil bearing capacity factor, and γ is the soil unit weight. Poisson's ratio for at-rest conditions υ_o, is:

$$\upsilon_o = \frac{K_o}{1 + K_o} \quad (2)$$

The soil bearing capacity factor, N_γ, according to the Rankine wedge theory, is:

$$N_\gamma = \tan(45 + \phi'/2)[\tan^4(45 + \phi'/2) - 1] \quad (3)$$

where ϕ' is the effective stress friction angle. As shown in Fig. 3, the value of the induced stress due to compaction operation significantly varies with the soil backfill friction angle. The reader is directed to the paper by Ehrlich and Mitchell (1994) for details about the derivation of the equations.

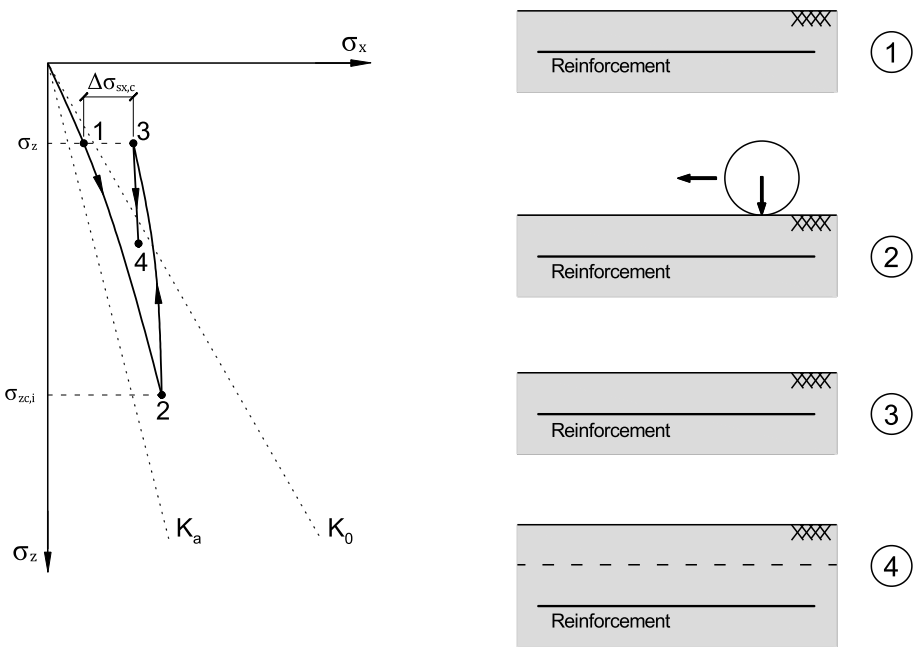

Fig. 1. Assumed stress path due to compaction of soil backfill layer. (1) Soil layer placement; (2) compaction equipment operation; (3) end of compaction; (4) next soil layer placement.

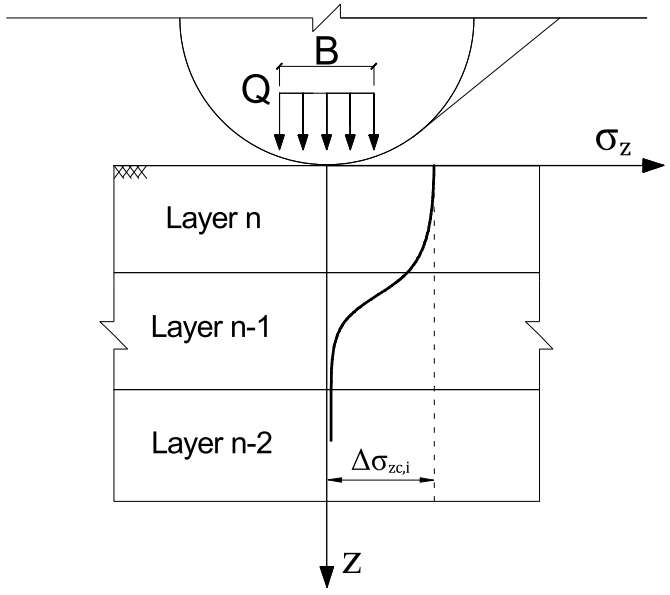

Fig. 2. Vertical stress increase during a roller operation in the backfill (strip load; Boussinesq elastic solution).

Table 1
Characteristics of various vibrating roller compactors (after Ehrlich and Becker, 2010).

Manufacturer	Model	Weight, kN	Width, m	Equivalent static load, kN	Vertical stress, kPa
CASE	SV212	72.3	2.20	277	*
MÜLLER	VAP55P	-	1.68	190	*
	VAP70P	-	2.14	320	*
DYNAPAC	CA134PD	19.6	1.37	89	*
	CA150PD	39.2	1.68	143	*
	CA250PD	72.6	2.13	300	*

*See Fig. 3.

Table 2
Characteristics of rammer compactors (after Ehrlich and Becker, 2010).

Manufacturer	Model	Equivalent static load, kN	Base area, m^2	Vertical stress, kPa
DYNAPAC	LT500	10.0	0.076	132
	LT600	14.8	0.092	160
	LT700	18.6	0.092	201
WACKER	BS 50-4	14.7	0.092	159
	BS 60-4	15.6	0.092	169
	BS 70-2i	17.8	0.092	193

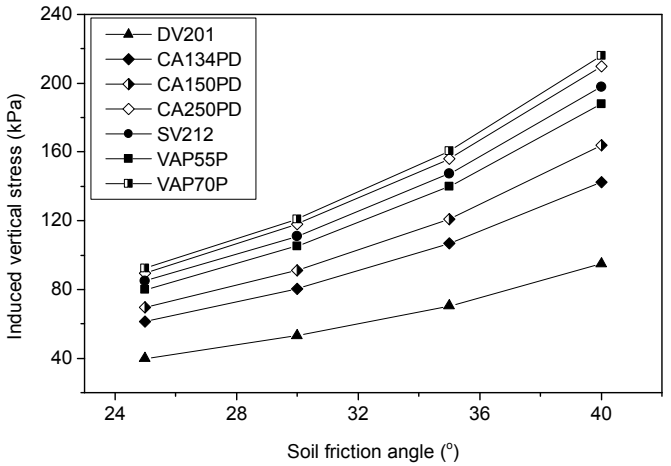

Fig. 3. Vertical stress induced by several compactor rollers (after Ehrlich and Becker, 2010).

3. Numerical model

The numerical modelling was performed using the 2D finite-element computer program PLAXIS (Brinkgreve and Vermeer, 2002). Data used for the validation of the analyses was obtained from a full-scale reinforced soil wall (wall 1) built at the Royal Military College of Canada (RMC) (Hatami and Bathurst, 2005).

Fig. 4 shows the geometry of the numerical model adapted from the

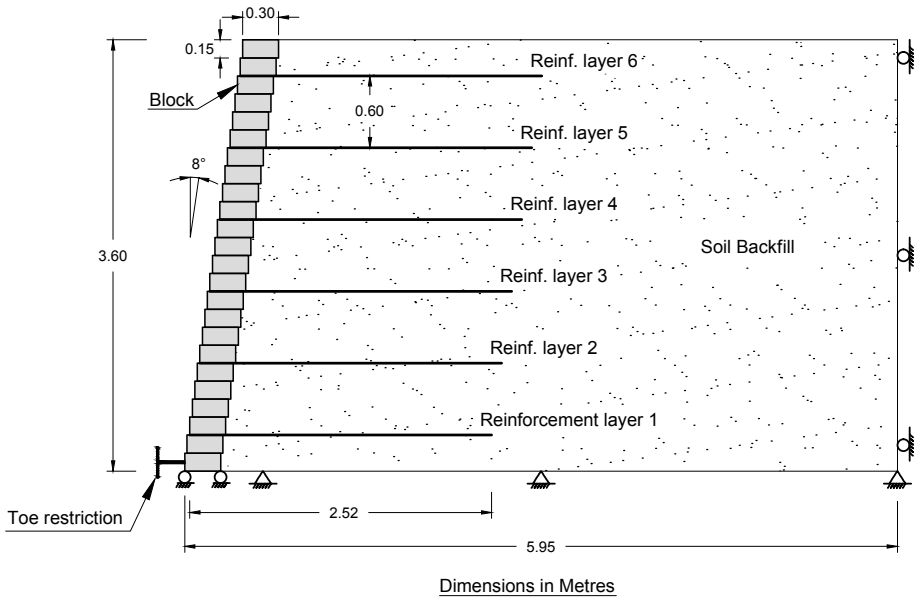

Fig. 4. Geometry of the numerical model validation adapted from the full-scale test.

full-scale test. The wall was 3.6 m high, with a facing inclination of 8° to the vertical. The length and vertical spacing of the geogrid were 2.52 m and 0.6 m, respectively. The input parameters were the same as those used by Guler et al. (2007). A hardening soil model, i.e. a hyperbolic soil model like the model of Duncan and Chang (1970), was applied. Hyperbolic stress-strain curves were arranged to fit measurements from the laboratory plane strain tests reported by Hatami and Bathurst (2005). A good match was shown for confining pressures equal to 20 kPa and 30 kPa, and for strain less than 1.5%, all of which are reasonable assumptions based on working stress conditions. The PLAXIS default value of $E_{ur}^{ref} = 3E_{50}^{ref}$ was used. E_{50}^{ref} and E_{ur}^{ref} are a reference stiffness modulus and the reference Young's modulus for unloading and reloading, respectively, corresponding to the reference confining pressure p^{ref}. The amount of stress dependency is given by the power *m*. In order to simulate a logarithmic stress dependency, as observed for soft clays, the power should be taken equal to 1.0 (Brinkgreve and Vermeer, 2002). Janbu (1963) reports values of *m* around 0.5 for Norwegian sands and silts, which was employed in the analysis. R_f is the failure ratio, which is taken as 0.9.

Reinforcement was modelled as a linear elastic material with perfect interface adherence to the adjacent soil. Dyer and Milligan (1984) and Jewell (1980) showed that perfect adherence is a reasonable assumption for a soil-reinforcement interface under working stress conditions. Parameters used to characterise block-block and soil-block interfaces were the same as those used by Guler et al. (2007). Fifteen-node triangular elements were used to model the soil layers and other volume clusters, and a fine mesh was used to divide the system into discrete segments for study. The types of structural elements and interfaces were assumed to be compatible with the soil element type. Table 3 shows the input parameters from the full-scale test wall used in this study.

The wall was constructed in stages; i.e. 0.15 m thick soil lifts were placed and compacted until the final wall height was reached. A fixed boundary condition in the horizontal direction was applied to the right lateral border. At the bottom of the model, a fixed boundary condition in both the horizontal and vertical directions was employed, except at the base of the block facing; at this point, a roller was modelled to allow only horizontal displacement. The horizontal toe reaction was measured in the physical model using a load ring. For the simulation of the toe condition, the bottom of the block facing was vertically restricted, and a horizontal fixed-end anchor with 4000 kN/m/m axial stiffness was used.

Table 3
Input parameters from the full-scale wall.

Property	Value
Soil properties	
Model	HS
Peak plane strain friction angle, ϕ (°)	44
Cohesion, *c* (kPa)	1.0
Dilation angle, Ψ (°)	11
Unit weight, γ (kN/m^3)	16.8
E_{50}^{ref}, (kPa)	56,667
E_{ur}^{ref}, (kPa)	170,000
Stress dependence exponent, m	0.5
Failure ratio, R_f	0.9
Poisson's ratio, υ	0.25
P_{ref}, (kPa)	80
Reinforcement	
Elastic axial stiffness (kN/m)	97
Modular block properties	
Model	Linear elastic
Size (m × m)	0.30 × 0.15 (length × height)
Unit weight, γ (kN/m^3)	21.8
Stiffness modulus (kPa)	1×10^6
Poisson's ratio, υ	0.15
Block-block interface	
Friction angle (°)	57
Cohesion (kPa)	46
Soil-block interface	
Friction angle (°)	44
Cohesion (kPa)	1
Dilation angle, Ψ (°)	11
Toe condition	
Axial stiffness of anchor (kN/m/m)	4000

4. Numerical modelling of compaction

Different methods were employed for modelling the compaction-induced stress as follows:

I) Applying a uniform vertical stress to the top of each backfill soil layer as the wall was being modelled from the bottom up, as suggested in the literature (e.g. Hatami and Bathurst, 2005) (referred to as procedure type I, see Fig. 5a).
II) Applying a distribution load at the top and bottom of each soil layer, as suggested by Mirmoradi and Ehrlich (2015a) (referred to as procedure type II, see Fig. 5b).

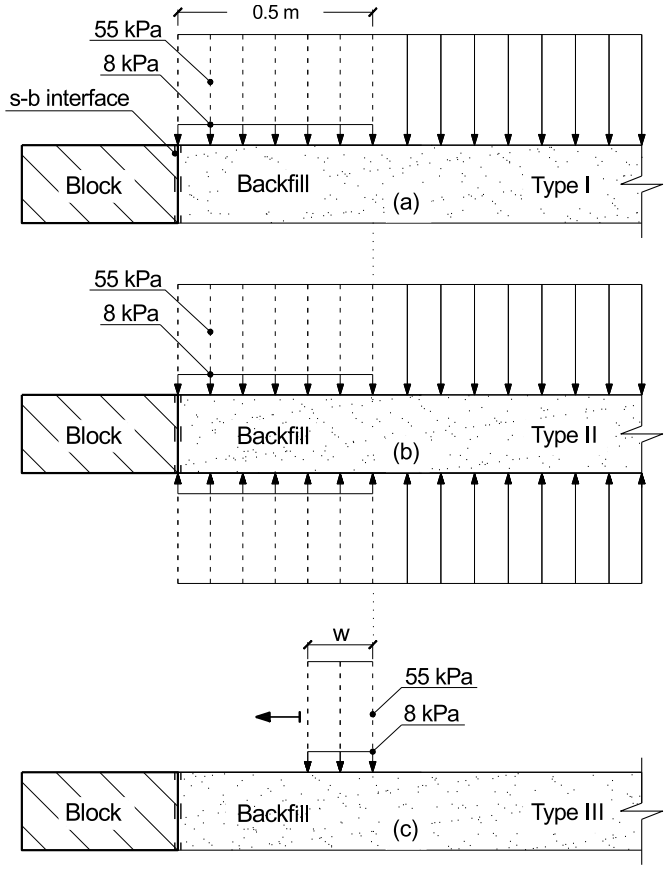

Fig. 5. Compaction procedures employed in the numerical analyses.

III) Modelling was also performed using different widths of strip load applied to the top of each backfill layer as the wall was being built from the bottom up. Three different widths of strip loads, w, are considered in this study: 0.5 m, 0.25 m, and 0.125 m (hereafter referred to as procedure type III, see Fig. 5c).

Regarding the compaction condition of the physical model considered in this study (wall 1), it should be mentioned that the first 0.5 m directly behind the wall-facing was hand-tamped to a target 95% of standard Proctor density, using a rigid steel plate to minimise construction-induced outward deformation and lateral stresses against the back of the facing. The backfill located beyond 0.5 m of the facing was compacted in 150 mm lifts using three passes of a walk-behind, gasoline-powered, vibrating-plate compactor (Whacker VPG-155A) with a dynamic contact pressure of 55 kPa (Bathurst et al., 2009).

For the numerical modelling of compaction, two conditions were considered, as shown in Fig. 5: A) The vertical stress used to model the CIS in the first 0.5 m behind the facing was 8 kPa, and the value of 55 kPa was employed for the backfill located beyond 0.5 m of the facing; B) The value of 55 kPa was applied to the entire surface of the backfill (including the first 0.5 m behind the facing). These two conditions have been considered in all the analyses using the different procedures employed for modelling CIS, i.e. types I, II, and III.

Fig. 6 shows three different approaches for the simulation of the induced stress due to compaction. Fig. 6a, b, and c show a schematic view of the numerical modelling of compaction-induced stress using a distributed load, q_c, at the top of each soil layer (type I); distribution loads, q_c, at the top and bottom of each soil layer (type II); and a strip load applied at the top of each soil backfill layer (type III), respectively. Stage construction is used in all procedures, and compaction modelling is represented by only one cycle of loading and unloading for each soil layer. In Fig. 6, four steps for backfill soil construction in a specific soil layer, n, were considered: (I) soil layer placement, (II) compaction equipment operation, (III) end of compaction, and (IV) next soil layer placement (layer $n + 1$). Fig. 6a, step (II) shows that when procedure type I is used for numerical modelling of the induced stresses due to compaction in soil layer n, it leads to a constant increase in the vertical stress due to compaction, q_c, in all layers below. The dashed line in this figure shows the expected vertical stress increased during the roller operation for soil layer n based on the strip load elastic solution, where its maximum value takes place at soil-roller contact and decreases significantly with depth. This figure clearly shows that using the distribution load solely at the top of each soil layer when modelling compaction cannot match the actual field conditions represented by the elastic solution.

Fig. 6b shows a schematic view of procedure type II, as suggested by Ehrlich and Mirmoradi (2013) and Mirmoradi and Ehrlich (2015a) for the numerical simulation of the induced stress due to compaction. Fig. 3b, step (II) shows that when procedure type II is used for the soil layer n, all points in this soil layer would be driven to the same vertical stress increase. In addition, for the soil layers placed under this layer, only geostatic stresses occur. A comparison between the curves related to the compaction modelling using procedure type II, and the dashed line represented by the elastic solution, indicates that this procedure may be more representative of the actual induced vertical stress during roller operation.

Fig. 6c illustrates a schematic view of procedure type III for the numerical modelling of CIS. This procedure would lead to the same pattern of vertical stress increase with depth as that represented by the elastic solution. Fig. 6c, step (II) shows that when procedure type III is employed, depending on the width of the strip load, the same vertical stress increase may occur in all soil layers. The width of the strip load assumed in the model should be representative of the soil-roller (or soil-plate) contact. If a representative dimension is considered, this procedure may correctly simulate the actual induced vertical stress during the operation of the compaction equipment.

5. Results and discussion

The results of the numerical analyses were compared with the measurements presented by Hatami and Bathurst (2005). Fig. 7a and b compares the measured values of the reinforcement strains at the end of construction with those determined by PLAXIS when considering compaction conditions “A” and “B”, respectively. Note that in condition “A” the CIS was simulated in the first 0.5 m behind the facing using a vertical stress value of 8 kPa, and a value of 55 kPa was employed for the backfill located beyond 0.5 m of the facing. In condition “B” a value of 55 kPa was applied to the entire surface of the backfill, including the first 0.5 m behind the facing. In Fig. 7, the results correspond to numerical analyses of the different procedures used for modelling CIS; i.e. type I, type II, type III-0.5 m, type III-0.25 m, and type III-0.125 m.

Fig. 7 shows that the reinforcement strains determined by PLAXIS using compaction procedure type I are significantly higher than the measured reinforcement strain distributions in all reinforcement layers. This is more pronounced for compaction condition “B”. Fig. 7 also illustrates, in general, a good agreement between the measured and calculated values of the reinforcement strains when compaction procedure type II was employed. This is with the exception of reinforcement layers 2 and 3, in which the measured reinforcement strains were higher than those calculated by PLAXIS using CIS modelling type II. Furthermore, Fig. 7 indicates that the reinforcement strains determined by PLAXIS, using compaction procedure type III, depend on the width of the strip load used to model the CIS. As expected, the results of the numerical analyses show that an increase in the width of the strip load, w, when simulating CIS, leads to a higher reinforcement strain distribution in all reinforcement layers. Using the 0.5 m-wide vertical strip load (type III-0.5 m), the numerical analyses over-predict the reinforcement strain distributions in all reinforcement layers, compared

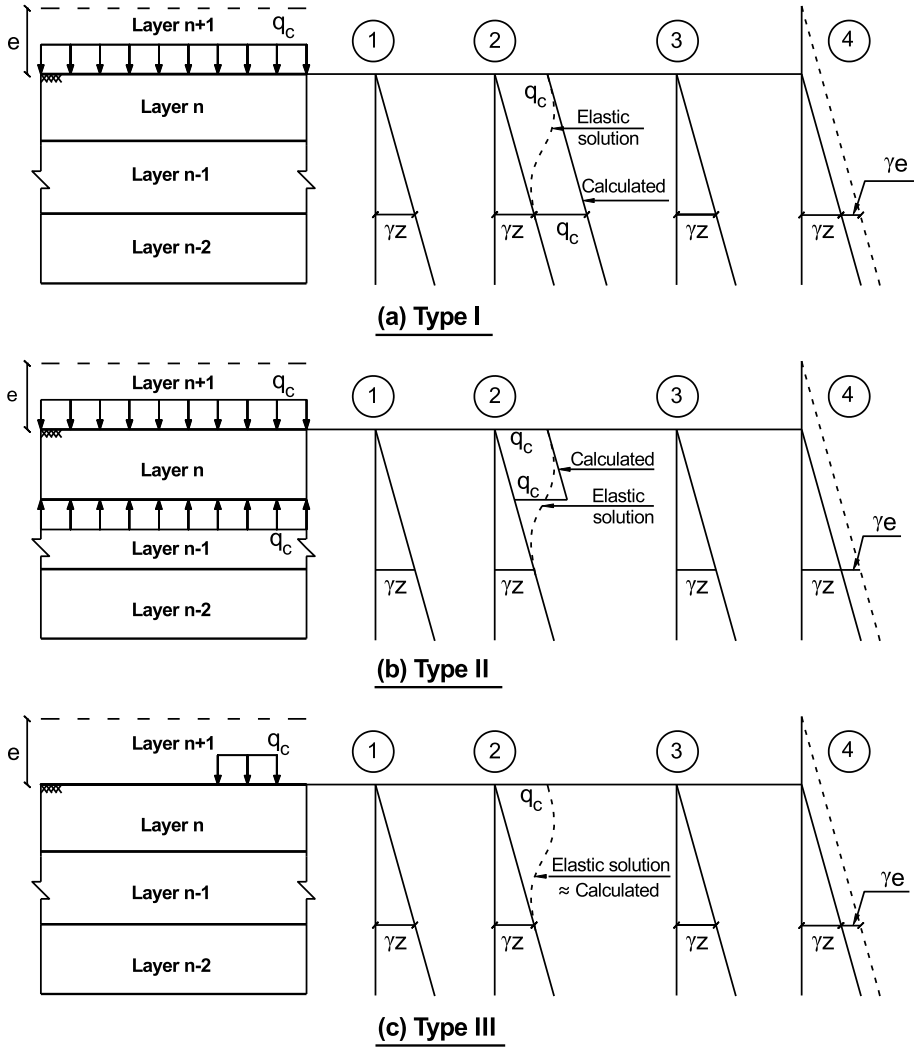

Fig. 6. Modelling of the vertical stress load–unload cycles verified during the compaction of the soil backfill layer, using different compaction procedures.

with the measurements. Nevertheless, the curves related to the models using compaction procedures type II and type III-0.125 m are very similar, and show satisfactory agreement between the calculated and measured reinforcement strains.

Comparison between Fig. 7a and b shows that the values of the reinforcement strains, especially close to the back of the block facing, increase for the models in which the entire backfill soil was compacted using the value of 55 kPa, i.e. compaction condition “B”. Moreover, in the models with this compaction condition, irrespective of the type of compaction procedure, the maximum reinforcement strain occurs close to the back of the block facing—except in reinforcement layer 1.

Fig. 8a and b compares the measured values of the connection load with those calculated by PLAXIS using compaction procedures type I, II, and III using compaction conditions “A” and “B”, respectively. The results show that the connection loads calculated by PLAXIS using compaction procedure type I were dramatically higher than the measurements in all reinforcement layers. Considering the different reinforcement layers, the average connection load calculated by PLAXIS using procedure type I for the conditions “A” and “B” were more than six and nine times those measured, respectively.

Fig. 8 shows that the measured values of the connection loads were reasonably well predicted by PLAXIS when compaction procedure type II was employed, except for in the first two layers near the bottom of the wall. This overestimation in the results of numerical studies were also observed in previous studies (e.g. Mirmoradi and Ehrlich, 2015b; Hatami and Bathurst, 2005).

Fig. 8 also demonstrates good agreement between the results of the numerical analyses using compaction procedure type III in which smaller widths of strip loads were employed, i.e. 0.25 m and 0.125 m. However, the connection load values calculated by PLAXIS for the model using compaction procedure type III-0.5 m were significantly higher than those measured, and this is more pronounced for the model in which compaction condition “B” was utilised (Fig. 8b). Furthermore, a comparison of Fig. 8a and b shows that, irrespective of the type of compaction procedure, the values of the connection loads are greater in the numerical analyses in which a value of 55 kPa was employed in the first 0.5 m behind the block facing (compaction condition “B”).

Fig. 9 shows a comparison between the calculated and measured values of the horizontally-facing displacement at the end of construction. The error bars in Fig. 9a and b indicate the range of deflection readings from two displacement potentiometers at each elevation, and ± 1 standard deviation on the measured loads (Hatami and Bathurst, 2005). Hatami and Bathurst (2005) stated that the measured values of facing displacements should not be confused with actual wall deformation profiles at the end of construction, because the measured values represent the lateral displacement of the block face recorded after the installation of the instruments through the end of construction.

Fig. 9 shows, in general, a similar trend to that observed in the previous results. A comparison between the measurements and the values calculated by PLAXIS using compaction procedure type I show that this modelling setup leads to significantly greater facing displacement values. The results again show that the measured values of the

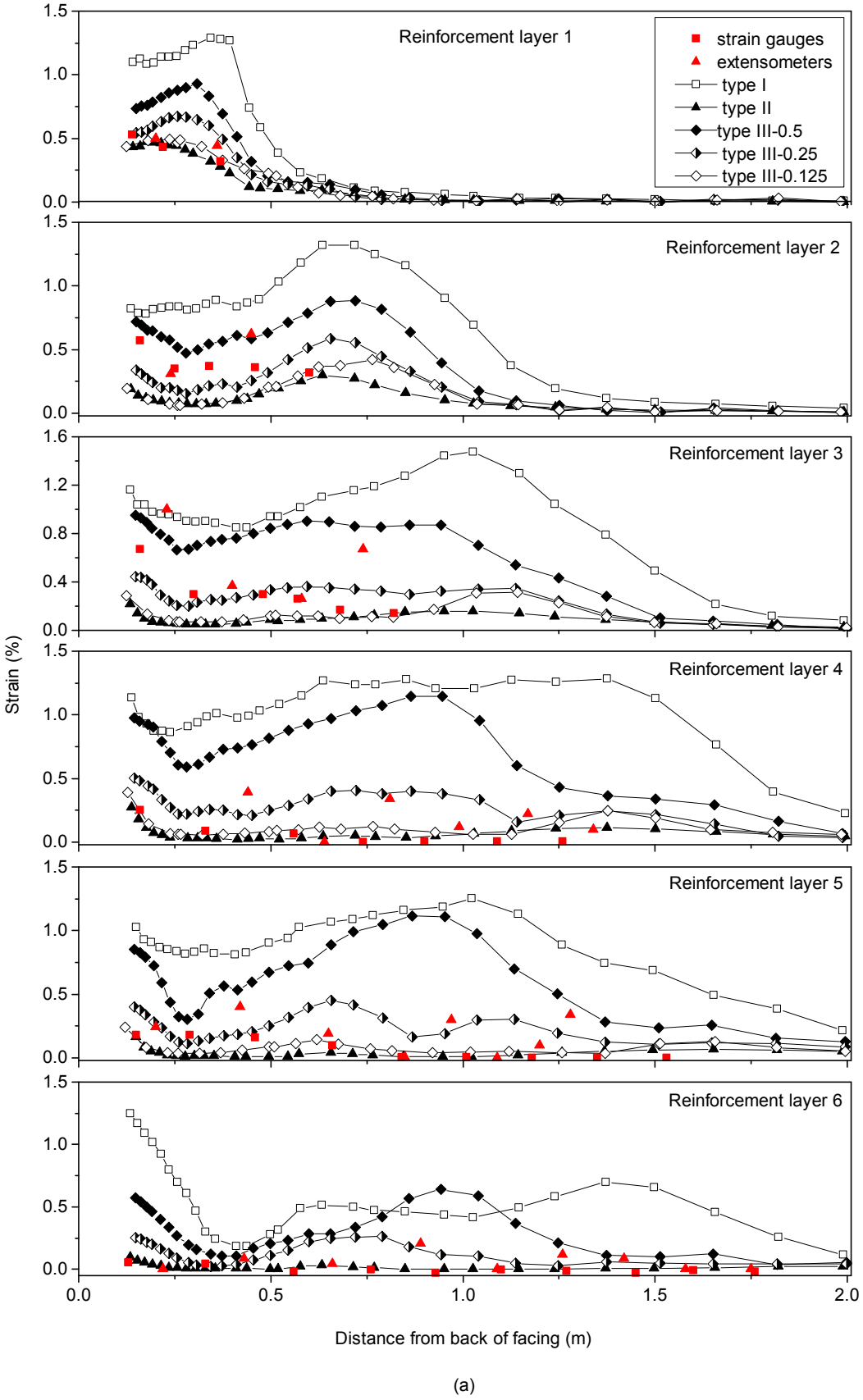

Fig. 7. Measured and calculated values of reinforcement strains using different compaction modelling at the end of construction: a) 0.5 m light compaction (condition "A"); b) 55 kPa compaction applied to the entire surface (condition "B").

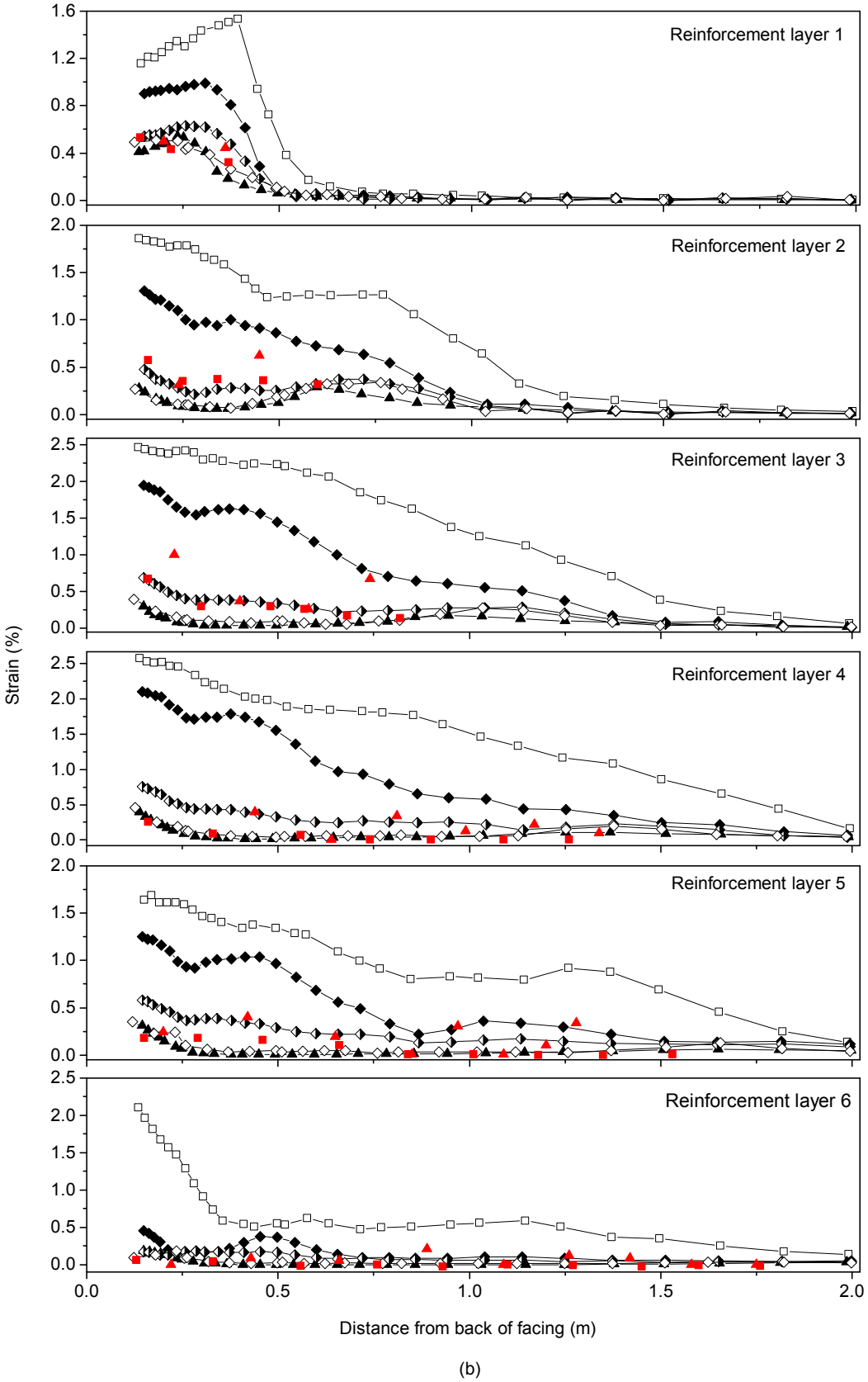

(b)

Fig. 7. (*continued*)

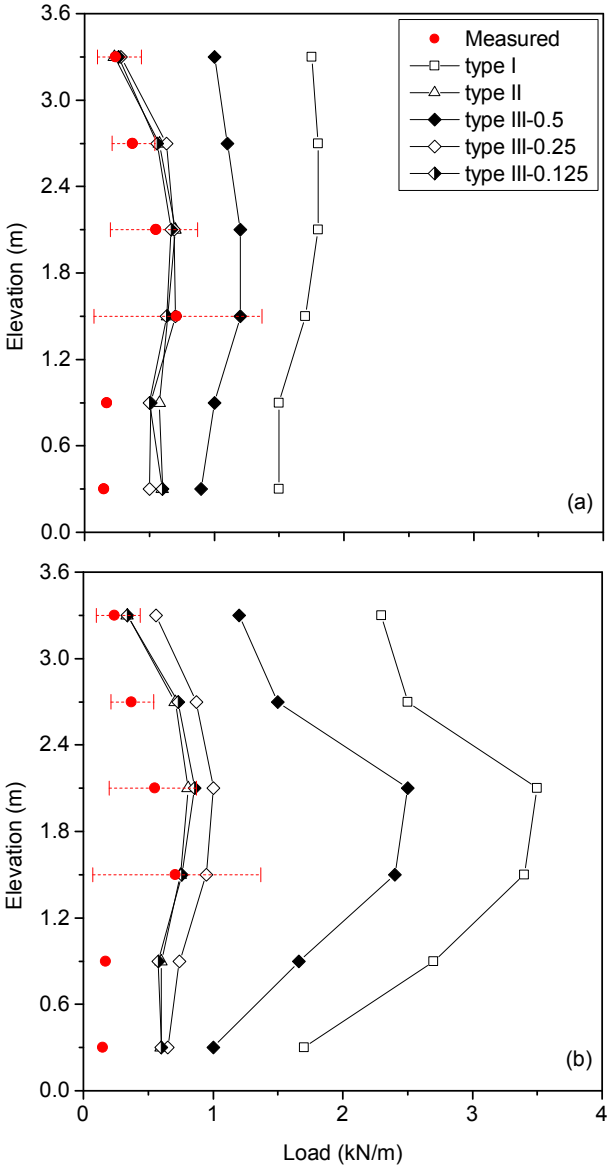

Fig. 8. Measured and calculated values of connection loads: a) 0.5 m light compaction (condition "A"); b) 55 kPa compaction applied to the entire surface (condition "B").

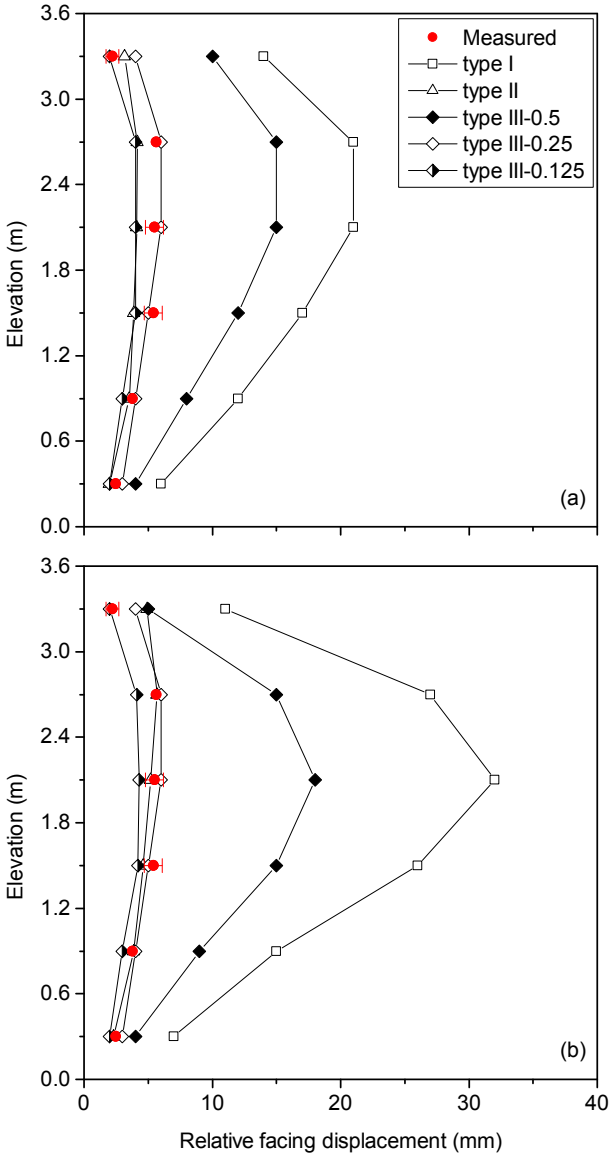

Fig. 9. Measured and calculated values of the horizontally-facing displacement at the end of construction: a) 0.5 m light compaction (condition "A"); b) 55 kPa compaction applied to the entire surface (condition "B").

facing displacement were reasonably well predicted by PLAXIS when compaction procedure type II was employed.

Moreover, when compaction procedure type III with a 0.5 m-wide strip load was employed to compaction simulation type III-0.5, the results were higher than those measured for both compaction conditions "A" and "B". Nevertheless, when using compaction types III-0.25 and III-0.125, satisfactory agreement between the calculated and measured facing displacement values are observed.

Fig. 10 shows comparisons between the measured and calculated values of the vertical and horizontal toe reactions in all stages. The numerical analyses are related to the different compaction procedures, and to compaction conditions "A" and "B". Relating to the different types of compaction modelling used in the analyses, the values of horizontal toe reaction determined by PLAXIS show a similar trend to the previously presented values of the reinforcement strains, connection loads, and facing displacements. The results show that the values of the horizontal toe reaction calculated by PLAXIS when compaction procedure type I was used were notably higher than the measured values. This is more noticeable in the results of the numerical analyses in which 55 kPa of vertical stress was applied to the entire surface of the backfill (Fig. 10b).

Fig. 10 also shows that, using compaction procedure type II, the results of the numerical modelling agree well with the measurements. In addition, when compaction procedure type III was employed, the accuracy of the results depended on the width of the strip load used in the modelling of CIS. This accuracy increased considerably with a decrease in the width of the strip load. Using compaction procedure type III-0.125, the numerical analyses reasonably predicted the measured values of the horizontal toe reaction in all stages. Furthermore, a comparison of Fig. 10a and b—related to the compaction conditions "A" and "B"—show that the main differences between the values of the horizontal toe reactions are related to the initial stages. For the models in which a value of 55 kPa was applied to the entire surface of the back of the block facing—condition "B"—the results show larger values of the horizontal toe reaction in the initial stages of the construction.

Moreover, Fig. 10 indicates that the numerical analyses using different procedures for modelling CIS reasonably predicted the measured values of the vertical toe reaction. Nevertheless, when compaction procedure type I was employed, the results show significantly lower values of vertical toe reaction calculated by PLAXIS, compared with the

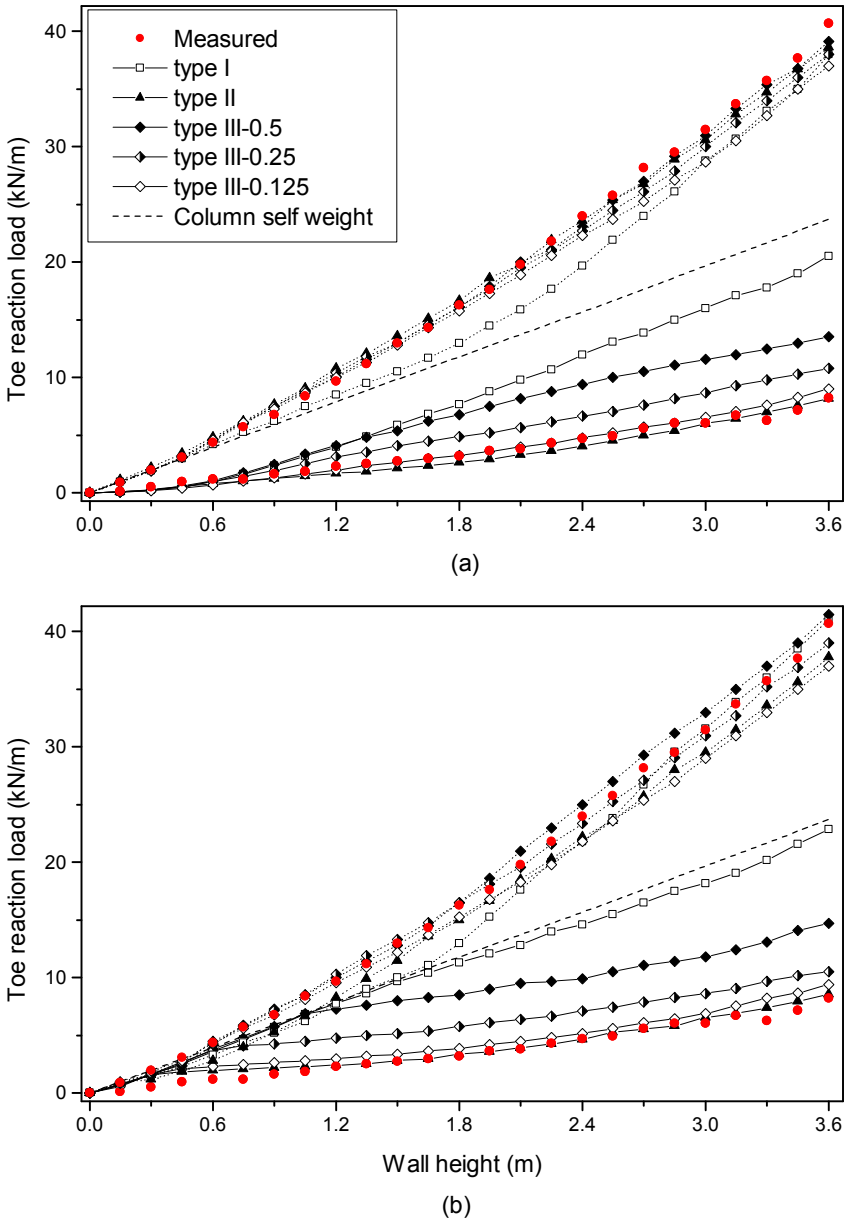

Fig. 10. Measured and calculated values of the vertical (dotted lines) and horizontal (solid lines) toe reactions in all stages: a) 0.5 m light compaction (condition "A"); b) 55 kPa compaction applied to the entire surface (condition "B").

measurement in the middle stages.

Fig. 11 shows the measured and predicted distributions of vertical contact pressures at the base of the wall. The values presented in this figure are normalised against the vertical pressure due to soil self-weight, $\gamma_s H$, where γ_s is the soil self-weight, and H is the height of the wall. Fig. 11a and b illustrate reasonable predictions of the foundation contact pressure determined by PLAXIS, considering different compaction procedures. The results indicate that, irrespective of the type of compaction modelling used in the numerical analyses, except for a local reduction behind the block facing, the foundation contact pressure is almost constant, with a magnitude corresponding to the soil depth. This means that the type of compaction modelling may not influence the distributions of vertical contact pressures at the base of the wall.

6. Conclusions

A numerical modelling of a geosynthetic-reinforced soil (GRS) wall was carried out using the data from a full-scale GRS segmental wall built at the Royal Military College of Canada RMC (wall 1). It should be noted that although the measured data used in this study (wall 1) have been already utilised for validation in several other numerical model studies, in none of those studies were the real value of the compaction specified for the vibrating plate compactor used in wall 1 employed. In this study the real value of compaction (i.e. 55 kPa) was employed in the analyses. The results of the numerical analyses using different compaction modelling procedures were compared with the measured values of the vertical and horizontal toe reactions during all stages of wall construction, the horizontally-facing displacement, the connection load, reinforcement strains, and distributions of vertical contact pressures at the base of the wall.

Analysis of the results showed that the numerical analyses in which the compaction was modelled by applying a uniform vertical stress to the top of each backfill layer as the wall was being modelled from the bottom (compaction procedure type I) significantly overestimates the measured values of the reinforcement strains, connection loads, facing displacement, and horizontal toe reaction. As mentioned earlier, this type of compaction procedure has already been employed in several studies in which the same wall was used for the numerical modelling validation, and satisfactory agreements have been reported when comparing the results of the numerical analysis and measurements (e.g.

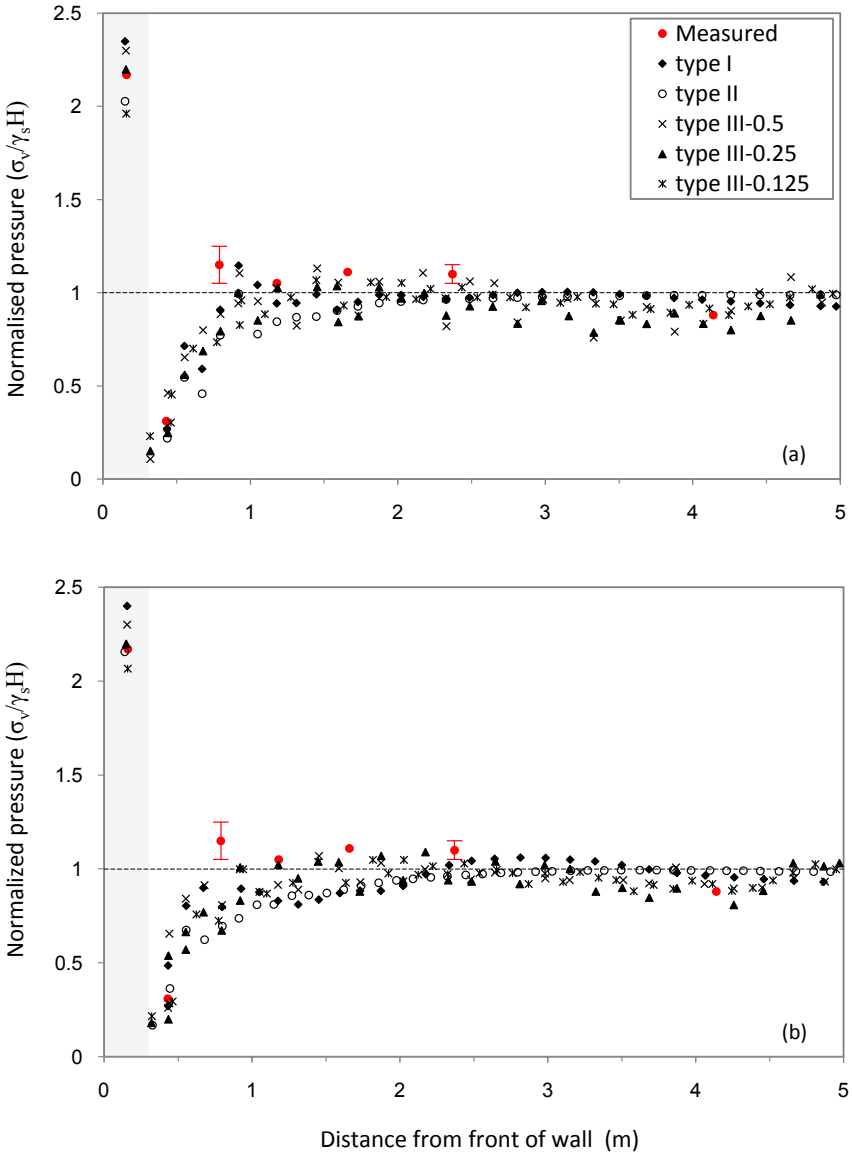

Fig. 11. Measured and predicted distributions of vertical contact pressures at the base of the wall: a) 0.5 m light compaction (condition "A"); b) 55 kPa compaction applied to the entire surface (condition "B").

Hatami and Bathurst, 2005; Ambauen et al., 2015; Yu et al., 2016, 2017). Nonetheless, it should be noted that in those studies the compaction value of 8 kPa was used in the numerical analyses, which is much less than the value specified for the compactor used in wall 1 (i.e. 55 kPa). Hatami and Bathurst (2005) stated that the value of 55 kPa was found to lead to excessive predictions of wall deflection when used as a uniform surcharge pressure across the entire soil surface. As clearly shown in the current study, this is due to the limitations of procedure type I for simulation of the compaction in actual field conditions.

When the compaction was simulated by applying a distribution load at the top and bottom of each soil layer (compaction procedure type II) satisfactory agreement has been generally observed between measurements and calculated values. Furthermore, for the numerical analysis in which the compaction was simulated using a strip load applied to the top of each backfill layer (compaction procedure type III), the accuracy of the results of the numerical analysis is dependent on the width of the strip load used. For the analyses in which lower widths of the strip loads were employed, i.e. 0.25 m and 0.125 m, good agreement between the calculated and the measured values were observed. Those results were also quite similar to those determined using compaction modelling type II. It should be mentioned that compaction modelling type III is time consuming. Therefore, from a practical point of view, it is suggested that procedure type II is used for the modelling of CIS.

Acknowledgements

The authors greatly appreciate the funding for this study provided by the Brazilian Federal Agency for Support and Evaluation of Graduate Education, CAPES, and the Brazilian Research Council CNPq (400538/2015-6).

References

AASHTO (American Association of State Highway and Transportation Officials), 2014. AASHTO LRFD Bridge Design Specifications, seventh ed. AASHTO, Washington, DC, USA.

Ambauen, S., Leshchinsky, B., Xie, Y., Rayamajhi, D., 2015. Service-state behavior of reinforced soil walls supporting spread footings: a parametric study using finite-element analysis. Geosynth. Int. 23 (3), 156–170.

Bathurst, R.J., Nernheim, A., Walters, D.L., Allen, T.M., Burgess, P., Saunders, D.D., 2009. Influence of reinforcement stiffness and compaction on the performance of four geosynthetic reinforced soil walls. Geosynth. Int. 16 (1), 43–59.

Brinkgreve, R.B.J., Vermeer, P.A., 2002. PLAXIS: Finite Element Code for Soil and Rock Analyses. CRC Press, Balkema, Leiden, Netherlands version 8.

BSI, 2010. BS 8006–1: Code of Practice for Strengthened/reinforced Soils and Other Fills. BSI, London, UK.

Duncan, J.M., Chang, C.Y., 1970. Nonlinear analysis of stress and strain in soils. J. Soil

Mech. Found. Div. 96 (5), 1629–1653.
Duncan, J.M., Seed, R.B., 1986. Compaction-induced earth pressures under Ko-conditions. J. Geotech. Engng. ASCE 112 (1), 1–22.
Dyer, N.R., Milligan, G.W.E., 1984. A photoelastic investigation of the interaction of a cohesionless soil with reinforcement placed at different orientations. In: Proc., Int. Conf. on in Situ Soil and Rock Reinforcement, pp. 257–262.
Ehrlich, M., Becker, L., 2010. Reinforced Soil Walls and Slopes: Design and Construction. Taylor & Francis, Abingdon, U.K.
Ehrlich, M., Mirmoradi, S.H., 2013. Evaluation of the effects of facing stiffness and toe resistance on the behavior of GRS walls. J. Geotextile Geomembr. 40 (Oct), 28–36.
Ehrlich, M., Mirmoradi, S.H., 2016. A simplified working stress design method for reinforced soil walls. Geotechnique 66 (10), 854–863.
Ehrlich, M., Mirmoradi, S.H., Saramago, R.P., 2012. Evaluation of the effect of compaction on the behavior of geosynthetic-reinforced soil walls. J. Geotextile Geomembr. 34, 108–115.
Ehrlich, M., Mitchell, J.K., 1994. Working stress design method for reinforced soil walls. J. Geotech. Eng. ASCE 120 (4), 625–645.
Ehrlich, M., Mitchell, J.K., 1995. Working stress design method for reinforced soil walls_closure. J. Geotech. Eng. ASCE 121 (11), 820–821.
Ehrlich, M., Mirmoradi, S.H., Xu, D.S., 2017. A simplified working stress design method for reinforced soil walls_Discussion. Geotechnique. https://doi.org/10.1680/jgeot.16.D.007.
Gu, M., Collin, J.G., Han, J., Zhang, Z., Tanyu, B.F., Leshchinsky, D., Ling, H.I., Rimoldi, P., 2017. Numerical analysis of instrumented mechanically stabilized gabion walls with large vertical reinforcement spacing. J. Geotextile Geomembr. 45, 294–306.
Guler, E., Hamderi, M., Demirkan, M.M., 2007. Numerical analysis of reinforced soil retaining wall structures with cohesive and granular backfills. Geosynth. Int. 14 (6), 330–345.
Hatami, K., Bathurst, R.J., 2005. Development and verification of a numerical model for the analysis of geosynthetic reinforced-soil segmental walls. Can. Geotech. J. 42 (4), 1066–1085.
Hermann, L.R., Al-Yassin, Z., 1978. Numerical analysis of reinforced soil systems. In: ASCE Symp. Earth Reinf, pp. 428–457 Pittsburgh, PA, USA.
Ho, S.K., Rowe, R.K., 1997. Effect of wall geometry on the behavior of reinforced soil walls. Geotext. Geomembranes 14, 521–541.
Janbu, J., 1963. Soil compressibility as determined by oedometer and triaxial tests. In: Proceedings of the European Conference on Soil Mechanics and Foundation Engineering, vol. 1. pp. 19–25 Wiesbaden.
Jewell, R.A., 1980. Some Effects of Reinforcement on the Mechanical Behavior of Soils. PhD thesis. Univ. of Cambridge, Cambridge, England.
Lambe, T.W., Whitman, R.V., 1969. Soil Mechanics. Wiley, New York.
Ling, H.I., Leshchinsky, D., 2003. Finite element parametric study of the behavior of segmental block reinforced-soil retaining walls. Geosynth. Int. 10 (3), 77–94.
Liu, H., Won, M.S., 2009. Long-term reinforcement load of geosynthetic-reinforced soil retaining walls. J. Geotech. Geoenviron. Eng. ASCE 135 (7), 875–889.
Mirmoradi, S.H., Ehrlich, M., 2015a. Modeling of the compaction-induced stress on reinforced soil walls. J. Geotextile Geomembr. 43 (1), 82–88.
Mirmoradi, S.H., Ehrlich, M., 2015b. Numerical evaluation of the behavior of GRS walls with segmental block facing under working stress conditions. ASCE J. Geotech. Geoenviron. Eng. 141 (3), 04014109.
Mirmoradi, S.H., Ehrlich, M., 2015c. Compaction-induced stress: numerical modeling. In: 15th Pan-American Conference on Soil Mechanics and Geotechnical Engineering, vol. XV PCSMGE, Buenos Aires, Argentina.
Mirmoradi, S.H., Ehrlich, M., 2014. Modeling of the compaction-induced stresses in numerical analyses of GRS walls. Int. J. Comput. Methods, Special Issue “Comput. Geomech. 11 (2) 1342002, 14 pages.
Mirmoradi, S.H., Ehrlich, M., 2016. Investigation of the prediction capability of the AASHTO simplified method under working stress conditions. In: 3rd Pan-American Conference on Geosynthetics, Miami, USA.
Rowe, R.K., Ho, S.K., 1993. Keynote lecture: a review of the behavior of reinforced soil walls. In: Ochiai, H., Hayashi, S., Otani, J. (Eds.), Earth Reinforcement Practice. Kyushu University, Fukuoka, Japan, pp. 801–830 November 1992, Proc. Int. Symposiumon Earth Reinforcement Practice, vol. 2. Balkema, Rotterdam, The Netherlands.
Scotland, I., Dixon, N., Frost, M., Fowmes, G., Horgan, G., 2016. Modelling deformation during the construction of wrapped geogrid-reinforced structures. Geosynth. Int. 23 (3), 219–232.
Yu, Y., Bathurst, R.J., Allen, T.M., 2016. Numerical modeling of the SR-18 geogrid reinforced modular block retaining walls. J. Geotech. Geoenviron. Eng. 142 (5), 04016003.
Yu, Y., Bathurst, R.J., Allen, T.M., 2017. Numerical modelling of two full-scale reinforced soil wrapped-face walls. J. Geotextile Geomembr. 45 (4), 237–249.